Control of Lateral Motions of the TERRAFOIL Transit Vehicle

J.E. Furman Jr.*
Boeing Aerospace Co., Seattle, Wash.
and
B.J. Hartz† and R.N. Clark‡
University of Washington, Seattle, Wash.

An active ride control system for the TERRAFOIL™ vehicle is described. The passenger compartment of this vehicle is supported above the roadway by long flexible struts, and its undercarriage is enclosed in an underground guideway. Lateral loads are imposed on the vehicle by cornering maneuvers, winds, and guideway roughness. This study shows that electrohydraulic servomechanisms designed to apply control moments at the base of the supporting struts can adequately confine the lateral motions of the passenger compartment within specified limits, even with extreme load disturbances. A dynamic model including the flexible strut shows the system to be controllable through the servovalve input signal and observable through feedback signals from the servopiston and an accelerometer mounted on the passenger compartment. Feedback control is achieved through a state estimator and an optimal control law matrix.

Nomenclature

ϕ = state variable associated with the passenger cab position, rads
Θ_p = state variable associated with the actuator platform rotation, rads
Θ_T = state variable associated with the undercarriage rotation, rads
x_s = state variable associated with the hydraulic spool valve position, m
γ = state variable associated with the hydraulic piston displacement and piston load pressure, m^3
g = acceleration of gravity, 9.81 m/sec^2 (32.2 fps^2)
U_s = strain energy of the flexible strut, Nt/m
$\boldsymbol{R}$ = strut displacement vector, 4×1
S = strut stiffness matrix, 4×4
L = strut length, 5.5 m (18.0 ft)
ℓ = radius of gyration of the actuator platform mass, 1.0 m (3.28 ft)
$\hat{L}$ = effective total vehicle height, 6.5 m (21.28 ft)
L_T = half the truck assembly's axle length, 0.9 m (3.0 ft)
L_p = half the distance between the hydraulic actuator chassis pivot points, 0.46 m (1.5 ft)
K_T = parallel combination of spring rates of one set of dual pneumatic tires, stabilizing wheel and supporting structure, 8.86×10^4 Nt/m (1.20×10^4 lb/ft)
EI = effective product of strut modulus of elasticity and area moment of inertia along the strut length, 1.6×10^7 Nt/m^2 (5.5×10^9 lb-in^2)
Q = total hydraulic fluid flow, liter/sec
Q_o = incompressible hydraulic fluid flow component, liter/sec
Q_c = compressible hydraulic fluid flow component, liter/sec
Q_L = actuator piston leakage flow component, liter/sec
P_s = constant hydraulic head pressure, 2.1×10^4 KPa (3×10^3 lb/in^2)
P_L = actuator piston load pressure, Pa
A_R = actuator piston effective area, 1.08×10^{-2} m^2 (16.7 in^2)
Y_R = actuator piston displacement, max travel of $\pm$ 0.076 m ($\pm$ 0.249 ft)
K_e = hydraulic line elastic coefficient, 0.0 liter/Pa-sec
K_L = actuator piston leakage coefficient, 0.0 liter/Pa-sec
k = effective spool valve orifice coefficient
x_o = servovalve spool underlap, m
v/K_B = hydraulic fluid elasticity coefficient, 2.38×10^{-12}m^5/Nt(.001 in^5/lb)
ω_n = servovalve nature frequency, 785 rads/sec
ζ = servovalve damping ratio, 0.78 rad
$K_A e$ = servovalve amplifier output voltage
M = half the mass of passenger cab and payload, 2.7×10^3 kg, (187 slugs)
M_P = mass of the actuator platform, 1.2×10^3 kg (82 slugs)
J_p = polar moment of inertia of the actuator platform, 757 kg-m^2
J_T = polar moment of inertia of chassis and truck assembly, 339 kg-m^2/strut (250 slug-ft^2/strut)
M_ϕ = external moment acting on the ϕ coordinate, Nt/m
M_{Θ_p} = external moment acting on the Θ_p coordinate, Nt/m
M_{Θ_T} = external moment acting on the Θ_T coordinate, Nt/m
W_ϕ = disturbance moment acting on the ϕ coordinate, Nt/m
W_{Θ_p} = disturbance moment acting on the $\Theta_p$coordinate, Nt/m
W_{Θ_t} = disturbance moment acting on the Θ_t coordinate, Nt/m
A = plant matrix, 9×9
$\boldsymbol{x}$ = plant state vector, 9×1
B = plant input matrix, 9×1
$\boldsymbol{u}$ = plant control vector, 1×1
C = system output matrix, 2×9
$\boldsymbol{y}$ = system output vector, 2×1
$\hat{\boldsymbol{x}}$ = estimated system state vector, 9×1
N = observer coordinate transformation matrix, 7×7

Received July 9, 1975; presented as Paper 75-1114 at the AIAA Guidance and Control Conference, Boston, Mass., Aug. 20-22, 1975; revision received Aug. 12, 1976.

Index categories: Navigation, Control, and Guidance Theory; Aerospace Technology Utilization.

*Senior Engineer.
†Professor of Civil Engineering.
‡Professor of Electrical Engineering. Associate Fellow AIAA.

q = plant state vector with respect to the observer coordinates
F = observer matrix, 7×7
z = observer state vector, 7×1
D = observer input matrix, 7×2
E = observer ouput matrix, 7×1
$\hat{q}$ = estimated plant state vector with respect to the observer coordinates
J = performance measure
Q_c = state variable weighting matrix, 9×9
R_c = control weighting matrix, 1×1
K = optimal control law matrix, 1×9
T = kinetic energy, Nt/m
V = potential energy, Nt/m
$\mathcal{L}$ = total Lagrangian

Introduction

THE TERRAFOIL is a new concept rapid transit vehicle.[1-3] The passenger compartment is supported above the surface traffic on two narrow struts in tandem, each of which is connected to the chassis. The chassis and undercarriage travel in an underground enclosed guideway with a narrow longitudinal slot for the supporting struts. Figure 1 shows a model of the proposed TERRAFOIL, and Fig. 2 shows the details of the undercarriage, support structure, and guideway.

The enclosed guideway is continuously supported underground so there is no lateral vehicle motion induced by guideway flexibility or dynamic response characteristics. However, because the passenger compartment is supported a considerable distance above the guideway to clear the surface traffic, it is susceptible to guideway roughness effects, lateral winds, and guideway curvature which can cause lateral motions of the compartment. It is desired to compensate for these affects with a servomechanism designed to apply control moments at the base of the struts to minimize the lateral motions of the passenger cab and to ensure stability and riding comfort. This control problem is therefore akin to similar dynamic problems encountered in control configured vehicles (CCV),[4-7] in hydrofoil boats,[8] and in heavy-lift helicopters (HLH).[9-10]

The two-axle chassis is designed to be torsionally flexible along its longitudinal axis, so that each axle is assumed to act independently for small longitudinal rotations of the axles. The passenger compartment is also designed as a torsionally flexible open channel section so that torsional coupling between the struts at their upper ends is also minimized. This coupling is further minimized because the vertical struts are of stressed-skin aircraft type construction so that almost all of the flexibility of the struts occurs at the bottom, in the narrow, high-strength plates connecting through the roadway slot to the undercarriage. Hence the rotations of the tops of the struts are very small. The inertial coupling between front and rear struts due to rotation of the passenger compartment about the vertical axis is also assumed to be small if the servosystem is working properly. Because of these properties we assume that the dynamic analysis of the lateral motions can be accomplished by treating each strut and its associated parts separately. Should there prove to be significant coupling between the two struts this interaction could be accomodated by appropriate cross-coupling of the servocontrol signals between front and rear. This is not done here, however.

Each truck assembly consists of a supporting frame which houses an axle with dual pneumatic tires, differential d.c. electric drive motor, guidance wheels, a set of stabilizing wheels (which trap the undercarriage in the guideway to prevent overturning), and the electrodydraulic servomechanism consisting of an electrically driven variable displacement pump, servovalves and their electronic drivers, and balanced push-pull hydraulic actuators providing a variable force and variable displacement link between an actuator platform on the strut base and the chassis frame. The

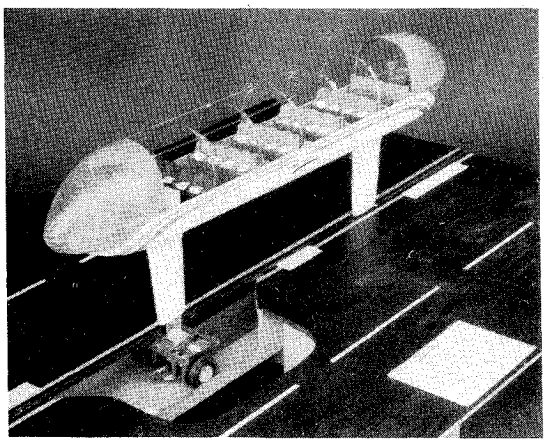

Fig. 1 Model of proposed TERRAFOIL vehicle.

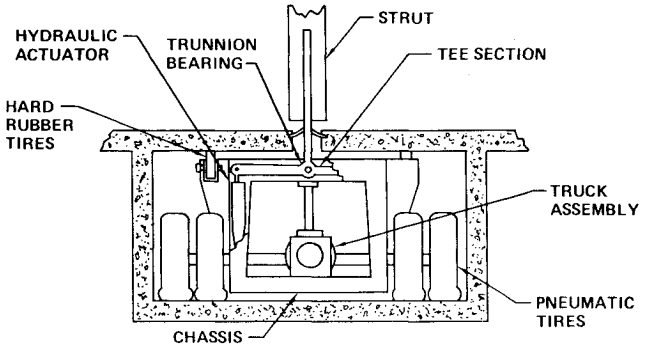

Fig. 2 Undercarriage and guideway configuration.

actuator platform is a high strength steel inverted tee section that joins the strut to the truck assembly. The tee is pinned to the supporting frame at the tee intersection (by a trunnion bearing) with the tee leg extending vertically upward through the slot in the guideway to join the strut. Hydraulic actuators are pinned between each tee end, and the truck supporting frame on each side such as to rotate the strut base when actuated.

The sensors for the lateral vehicle motion are an accelerometer to measure lateral accelerations of the passenger compartment at the top of each strut and piston displacement transducers at the actuators to measure strut base rotation relative to the truck assembly. It is shown in the subsequent sections of this paper that the lateral vehicle motions are controllable by this servosystem using these measurements and a state estimator with an optimal control law matrix.

The supporting struts are taken to be 5.5m (18 ft) long and their mass is lumped with the passenger compartment and actuator platform masses. The actuator platform mass is assumed to act at its point of rotation. The strut, pneumatic tire and actuator platform stiffness used are expected to approximate values for a realistic TERRAFOIL design for a 30 passenger transit vehicle.

Mathematical Model of the Lateral Axis Dynamics

Figure 3 shows the components considered in the analysis. These are the flexible strut, the passenger compartment, the hydraulic actuator system and the undercarriage mechanisms. Brief discussions of these components follow (a more detailed discussion can be found in Ref. 12).

Since the strut is of aircraft construction, its mass per unit length is negligible; therefore, the energy stored in the strut due to strut deflection is simply the strain energy of the strut, i.e., potential energy, and it may be expressed as a function of the boundary conditions over the strut surface. In deter-

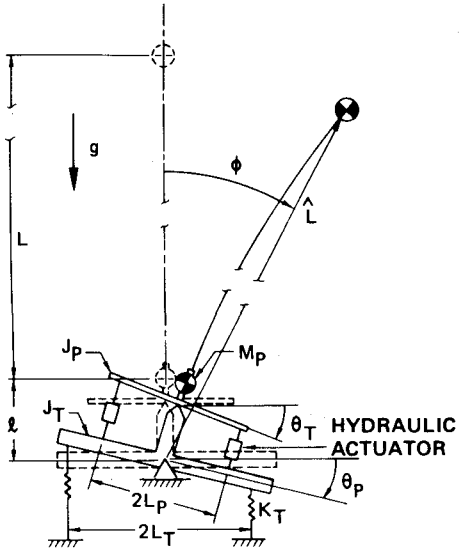

Fig. 3 Schematic of lateral axis dynamic elements.

mining this energy, the strut model need only relate the boundary conditions at one end of the strut to the boundary conditions at the other end. The boundary conditions at the passenger compartment consist of an axial compressive load due to the passenger compartment and payload weight, a lateral shear load due to lateral forces acting on the passenger compartment and strut, and a lateral bending moment due to the torsion carried by the passenger compartment. The compressive load transmitted to the strut by the passenger compartment contributes negligibly to the bending moment along the length of the strut and, therefore, need not be considered in the flexible strut model. The passenger compartment is structurally an open section, which implies that its ability to transmit torsion along its length is slight. Therefore, the lateral bending moment imposed on the strut due to the passenger compartment torsion may be ignored.

The boundary conditions at the bottom of the strut are imposed displacements. The axial displacement of the strut is constrained by the action of the stabilizing wheels. The only nonzero displacements at the bottom of the strut are the angular rotation of the actuator platform about the trunnion bearing and the lateral translation of the trunnion bearing due to the rotation of the undercarriage.

The strain energy can be written in terms of the displacements at each end of the strut. In matrix form the strain energy is

$$U_s = \tfrac{1}{2}\boldsymbol{R}^T\boldsymbol{S}\boldsymbol{R}$$

Since the lateral bending moment at the passenger compartment is zero, the strain energy stored in the strut reduces to

$$U_s = (3EI/2L^3)\ [\hat{L}^2\phi^2 + L^2\Theta_p^2 + \ell^2\Theta_T^2 - 2\hat{L}\ell\phi\Theta_T + 2L\ell\Theta_p\Theta_T - 2\hat{L}L\phi\Theta_p]$$

where

$$\hat{L} = L + \ell$$

The rotation of the chassis about the midpoint of the truck assembly, which is taken as the system reference, produces a kinematic translation of the actuator platform and trunnion bearing (the location of the trunnion bearing for simplicity is taken to be the center of mass of the actuator platform).

This chassis rotation stores spring potential energy via tire compression and inverted pendulum gravitational potential energy by the translation of the actuator platform mass. The kinetic energy storage due to chassis rotation is proportional to the sum of J_T and $M_p\ell^2$.

The linear dynamic model of the hydraulic actuator system consists of a servovalve model and an actuator model. The servovalve which was modeled is a two stage (flapper and spool valve) aircraft type valve. It is assumed that the components are properly matched and the servovalve is supplied by a constant pressure source. Therefore, this study will only reflect the effects of the servovalve and actuator cylinder flow characteristics on the TERRAFOIL lateral axis system dynamics.

The flapper stage of the servovalve consists of a set of electromagnets on either side of the flapper. The electromagnets are controlled by differential coil currents so that they operate in a push-pull fashion on the flapper. The windings of the electromagnets are in the output circuitry of the servovalve amplifier.

The dynamics of the torque motor and armature-flapper assembly are several orders of magnitude faster than those of the second stage, and therefore need not be considered.

The second stage of the servovalve is a four-way underlapped spool valve. The hydraulic flow through the valve can be expressed as a function of the supply pressure, the spool position, the load pressure, the effective spool-land orifice coefficient, and the spool valve underlap.

Since the piston displacement is small, the fluid flow from the spool valve to the cylinder and the returning flow are equal. This allows the fluid flow through the spool valve to be characterized as a single flow Q.

The first-order approximation to the spool valve flow can be derived by standard techniques[11, 14]; this leads to flow components due to spool position and load pressure.

Though the dynamics of the servovalve are of a higher order, for the valve modeled, the no-load frequency response curves show that second-order dynamics are sufficient.

The actuator consists of a piston and piston rod assembly enclosed in a rigid cylinder housing with spherical bearings located in the rod assembly and in the opposite end of the housing. Since the actuators will act in a push-pull fashion, they must be balanced cylindrical actuators, i.e., equal working areas on both sides of their piston faces. The dominant actuator dynamics will be the dynamics associated with the flow of hydraulic fluid through the actuator. The flow through the actuator is then composed of three fundamental components: incompressible flow, compressible flow, and piston leakage flow.

The equations of motion for the system model may be formulated by combining the equations obtained from the total Lagrangian with the constraints of the hydraulic actuator system model and undercarriage geometry. The total Lagrangian is $\mathcal{L} = T - V$ where

$$T = \tfrac{1}{2}M\hat{L}^2\dot{\phi}^2 + \tfrac{1}{2}J_p\dot{\Theta}_p^2 + \tfrac{1}{2}(J_T + M_p\ell^2)\dot{\Theta}_T^2$$

$$V = Mg\hat{L}\cos\phi + (3EI/2L^3)\ [\hat{L}^2\phi^2 + L^2\Theta_p^2 + \ell^2\Theta_T^2 - 2\hat{L}\ell\Theta_T + 2\hat{L}\ell\phi\Theta_T + 2L\ell\Theta_p\Theta_T - 2\hat{L}L\phi\Theta_p] + M_pg\ell\cos\Theta_T + K_TL^2{}_T\Theta^2{}_T$$

The equations obtained from the Lagrangian are:
for the ϕ coordinate

$$\ddot{\phi} = -\left(\frac{3EI\hat{L}^2 - Mg\hat{L}L^3}{M\hat{L}^2L^3}\right)\phi + \left(\frac{3EI}{M\hat{L}L^2}\right)\Theta_p + \left(\frac{3EI\ell}{M\hat{L}L^2}\right)\Theta_T + \frac{1}{M\hat{L}^2}M_\phi$$

for the Θ_T coordinate

$$\ddot{\Theta}_T = -\frac{3EI\ell^2 - M_p g\ell L^3 + 2K_T L^2{}_T L^3}{(M_p\ell^2 + J_T)L^3}\Theta_T - \frac{3EI\ell - 2K_p L_p{}^2 L^2}{(M_p\ell^2 + J_T)L^2}\Theta_p + \frac{3EI\hat{L}\ell}{(M_p\ell^2 + J_T)L^3}\phi + \frac{1}{(M_p\ell^2 + J_T)}M_{\Theta_T}$$

for the Θ_p coordinate

$$\ddot{\Theta}_p = -\frac{3EI}{J_p L}\Theta_p - \frac{3EI\ell}{J_p L^2}\Theta_T + \frac{3EI\hat{L}}{J_p L^2}\phi + \frac{1}{J_p}M_{\Theta_p}$$

The constraints of the hydraulic actuator system are:
for the spool valve dynamics

$$\ddot{x}_s = -2\zeta\omega_n\dot{x}_s - \omega^2{}_n x_s + K_A e$$

for the spool valve flow

$$Q = k\sqrt{\frac{P_s - P_L}{2}}\,x_s - kx_o\sqrt{\frac{2}{P_s - P_L}}\,P_L$$

for the actuator flow

$$Q = A_R\dot{Y}_R + [K_e + v/K_B]\dot{P}_L + K_L P_L$$

for the undercarriage geometry

$$Y_R = L_p(\Theta_T - \Theta_p)$$

The external moments acting on the independent coordinates are:

$$M_\phi = W_\phi$$

$$M_{\Theta_p} = -2L_p A_R P_L + W_{\Theta_p}$$

$$M_{\Theta_T} = 2L_p A_R P_L + W_{\Theta_T}$$

where W_ϕ, W_{Θ_p}, and W_{Θ_T} are disturbance moments.

The hydraulic flow equations may be linearized by making a change of variables and expanding in a Taylor series about the origin.

Let $\gamma = A_R Y_R + [K_e + (v/K_B)]P_L$, then expanding and dropping terms of orders higher than one of the flow equations reduces to

$$\dot{\gamma} = -\frac{1}{A_2}\left(\frac{k}{4}\sqrt{\frac{2}{P_S}} + A_3\right)\gamma + k\sqrt{\frac{P_S}{2}}\,x_s + \frac{A_1}{A_2}\left(\frac{kx_o}{4}\frac{\sqrt{2}}{P_S} + A_3\right)Y_R$$

where

$$A_1 = A_R \quad A_2 = (K_e + K_B/v) \quad A_3 = K_L$$

Controller Design

The linearized dynamic equations for the lateral axis of the vehicle and the electrohydraulic servoactuator may be combined into the standard state variable form

$$\dot{x} = Ax + Bu$$

where the state vector is:

$$x = [\phi \quad \dot{\phi} \quad \Theta_T \quad \dot{\Theta}_T \quad \Theta_p \quad \dot{\Theta}_p \quad \gamma \quad x_s \quad \dot{x}_s]^T$$

and the control vector, which is a scalar, is $u = e$.

The output vector is provided by two instruments, a position transducer at the actuator piston and a laterally mounted accelerometer at the level of the passenger compartment. The system output equations is, therefore

$$y = Cx = [\hat{L} \quad \ddot{\phi} \quad Y_R]^T$$

and the C matrix is

$$C = \begin{bmatrix} \hat{L}a_{21} & 0 & \hat{L}a_{23} & 0 & \hat{L}a_{25} & 0 & 0 & 0 & 0 \\ 0 & 0 & L_p & 0 & -L_p & 0 & 0 & 0 & 0 \end{bmatrix}$$

where a_{21}, a_{23}, and a_{25} are elements of the A matrix which are listed in the Appendix, along with those of the B matrix.

The controller design is based on the state estimator-optimal control law approach. A Leunberger observer is used to provide an on-line estimate of the state vector as shown in Fig. 4. From the estimated state vector $\hat{x}$ the control signal u is derived through the 1×9 control law matrix K, $u = K\hat{x}$.

The vehicle is completely state controllable and completely state observable with the A, B, and C matrices shown here. The nine eigenvalues of the A matrix are as follows: $-0.64 \pm j\,216$, $-0.07 \pm j\,4.13$, $-0.08 \pm j\,76.9$, $-613 \pm j\,491$, and $+0.01$. Note the single right half plane eigenvalue. This is due to the inverted pendulum characteristic of the suspended vehicle. If the control valve is open, this mode can be excited. If the control valve is shut, the inverted pendulum characteristic is exhibited by a lightly damped, but stable mode. The first bending mode for the strut also appears as one of these lightly damped pairs.

A reduced-order observer can be designed for this system using standard techniques.[13] The dynamic order of the observer is seven because the vehicle is ninth order and there are two linearly independent instruments. The eigenvalues of the observer were arbitrarily chosen to have real parts of -1800 and imaginary parts of 0, ± 600, ± 1200 and ± 1800. These locations were perhaps unnecessarily far into the left half plane because the convergence time for the observer need be short compared to the mission length and not compared to the time response of the vehicle, because once $\hat{x}(t)$ converges to $x(t)$ it will continue to track it, irrespective of the eigenvalues of the observer, provided only that these are in the left half plane, of course.

The dynamic equations of the observer are obtained following Luenberger's procedure.[13] Because the C matrix is not in the required form $[I \vdots 0]$ a change of coordinates is effected, $q = Nx$, so that the state variable equations in the q coordinates are

$$q = NAN^{-1}q + NBu$$

$$y = CN^{-1}q$$

and CN^{-1} has the desired form $[I \vdots 0]$. Thus the observer produces $\hat{q}$, an estimate of q, and this is converted to $\hat{x}$ at the output of the observer: $\hat{x} = N^{-1}\hat{q}$. The observer equations are of the form

$$\dot{z} = Fz + NBu + Dy$$

$$\hat{q} = E\begin{bmatrix} z \\ y \end{bmatrix}$$

where F is 7×7, D is 7×2, and E is 9×9. The elements of these matrices are derived to satisfy the eigenvalue placement and basic estimation requirements.[13]

The optimal control law matrix K was found to be $[-349 \quad 1047 \quad 2314 \quad -3.2 \quad -1490 \quad 4.7 \quad -17 \quad -360 \quad -0.6]$ using the following procedure. A standard quadratic performance

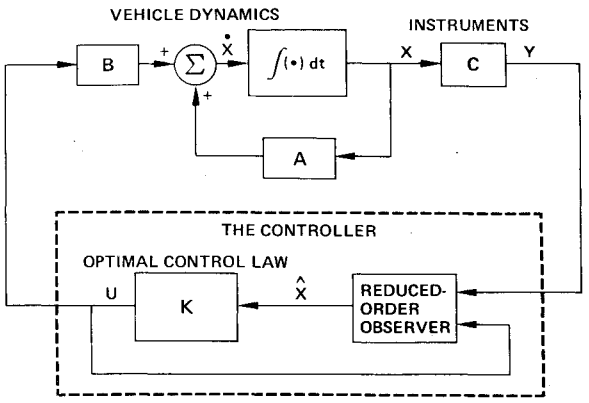

Fig. 4 System block diagram.

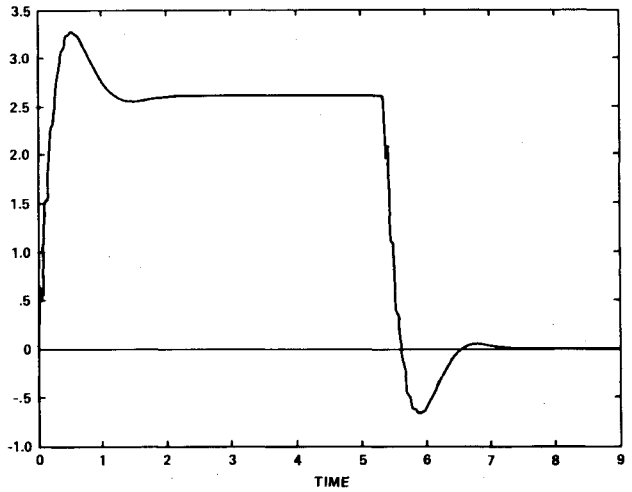

Fig. 5 Response to cornering maneuver, lateral acceleration of passenger compartment, m/sec^2.

function J was defined

$$J=\int_0^\infty [x^T Q_p x + u^T R_p u]\,dt$$

where $u=Kx$ and the elements of K were found such that J is minimized by standard techniques.[14] This was done for arbitrary values for the elements of the (positive definite) Q_p and R_p matrices and for initial values of the state variables corresponding to an impulse of lateral acceleration. This assures that the transient response to such an impulse would be optimal in this sense. Then the resultant K matrix was used in a transient test of the system subjected to a step disturbance of lateral acceleration, as described below. If the peak values of the various transients in the system exceeded their design levels, then changes were made in the Q_p and R_p matrices, a new K computed, and another transient test was run. This process was repeated until the resultant transient responses were acceptable. This curious approach combining both optimal design and trial and error procedures was feasible because the optimal design portion was completely automated by computer! Because of the separation principle the sixteen eigenvalues of the composite system are those of the observer plus those of the matrix $[A+BK]$, which turned out to be -900, -654, -160, $-30\pm j218$, $-2.72\pm j3.39$, and $-7.3\pm j75$.

System Simulation and Test Results

The transient tests were conducted via digital simulation. The tests simulated were a cornering maneuver and a lateral wind gust loading. The tests were chosen to be compatible with the ultimate vehicle design requirements. The cornering

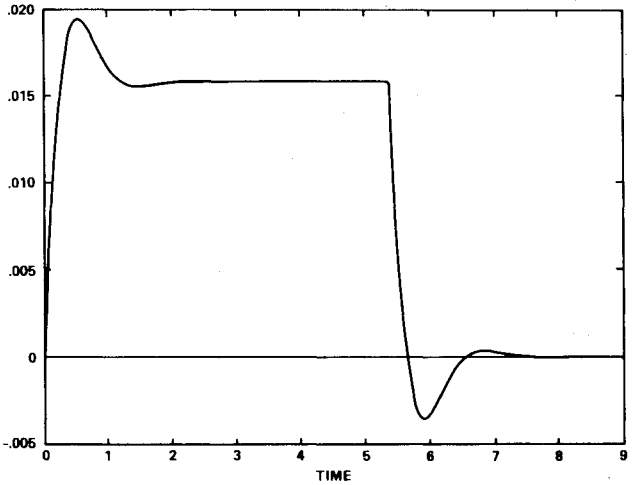

Fig. 6 Response to cornering maneuver, pneumatic tire deflection, m.

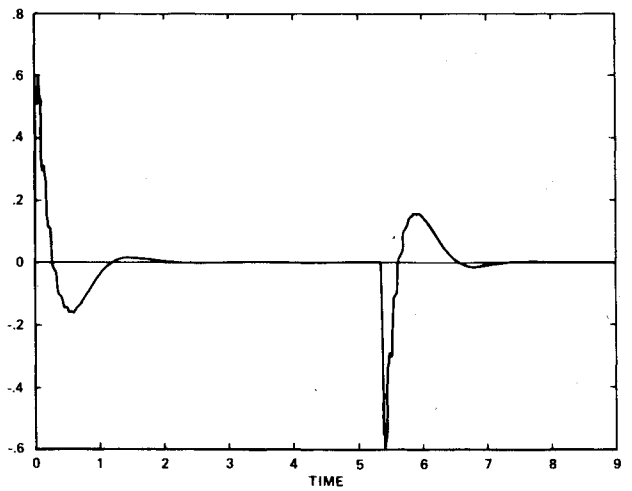

Fig. 7 Response to cornering maneuver, hydraulic fluid flow, l./sec.

maneuver was a ninety degree, 30.4 m (100 ft) radius turn without spiral transition or track banking. The vehicle speed was 9.0 m/sec (20 mph). The lateral gust loading was 44.7 m/sec (100 MPH) with a rise time of one second.

The cornering maneuver generates external moments on the ϕ and Θ_p coordinates due to the acceleration of the passenger compartment and actuator platform masses respectively. These moments, of course, increase with increasing ϕ and Θ_p. The lateral gust load generates an external moment on the ϕ coordinate only.

The peak transients of design interest are shown in Table 1. Figures 5, 6, and 7 show typical system transients. The transient tests show that the controller has stabilized all vehicle dynamic modes and adequately damped the inverted pendulum and strut bending modes. The vehicle's response to lateral loads is dominated by the inverted pendulum mode which has a damping ratio of 0.63.

For the cornering maneuver test, the peak passenger compartment acceleration transient is 24% greater than the steady state cornering acceleration. (This, of couse, could be greatly reduced by adding spiral corner transitions to the roadway). For the wind gust loading test, the max. hydraulic flow was 25% below the valve capacity. All peak undercarriage transients for both maneuvers were within the allowable physical constraints.

The peak transients of design interest are shown in Table 1. Figures 5, 6, and 7 show typical system transients. The transient tests show that the controller has stabilized all

Table 1 Peak transients

	Cornering	Gust load
Pass. comp. displacement	0.16 m	0.58 m
Tire deflection	0.02 m	0.06 m
$\hat{L}\ddot{\phi}$	3.3 m/sec^2	0.18 m/sec^2
Y_R	1.4×10^{-3}m	1.7×10^{-3}m
Q	$0.6L$/sec	$1.2L$/sec

vehicle dynamic modes and adequately damped the inverted pendulum and strut bending modes. The vehicle's response to lateral loads is dominated by the inverted pendulum mode which has a damping ratio of 0.63.

For the cornering maneuver test, the peak passenger compartment acceleration transient is 24% greater than the steady-state cornering acceleration. (This, of course, could be greatly reduced by adding spiral corner transitions to the roadway). For the wind gust loading test, the maximum hydraulic flow was 25% below the valve capacity. All peak undercarriage transients for both maneuvers were within the allowable physical constraints.

Appendix

Most of the elements of the A matrix are zero. Those which are not are

$$a_{12}=a_{34}=a_{56}=a_{89}=1$$

$$a_{21}=\frac{MgL^3-\alpha\hat{L}}{M\hat{L}L^3} \qquad a_{23}=\frac{\alpha\ell}{M\hat{L}L^3}$$

$$a_{25}=\frac{\alpha}{M\hat{L}L^2} \qquad a_{41}=\frac{\alpha\hat{L}\ell}{\epsilon L^3}$$

$$a_{43}=\frac{M_pg\ell L^3-2K_TL_T^2L^3-\alpha\ell^2}{\epsilon L^3}-\frac{2L_p^2A_R^2}{\epsilon\beta}$$

$$a_{45}=\frac{2L_p^2A_R^2}{\epsilon\beta}-\frac{\alpha\ell}{\epsilon L^2} \qquad a_{47}=\frac{2L_pA_R}{\epsilon\beta}$$

$$a_{61}=\frac{\alpha\hat{L}}{J_pL^2} \qquad a_{63}=\frac{2L_p^2A_R^2}{J_p\beta}-\frac{\alpha\ell}{J_pL^2}$$

$$a_{65}=-\frac{\alpha}{J_pL}-\frac{2L_p^2A_R^2}{J_p\beta} \qquad a_{67}=-\frac{2L_pA_R}{J_p\beta}$$

$$a_{73}=\frac{A_RL_p}{\beta}\left[\frac{kx_0}{4}\sqrt{\frac{2}{P_s}}+K_L\right] \qquad a_{75}=-a_{73}$$

$$a_{77}=-\frac{a_{73}}{A_RL_p} \qquad a_{78}=k\sqrt{\frac{P_s}{2}}$$

$$a_{98}=-2\zeta\omega_n \qquad a_{99}=-\omega_n^2$$

where $\alpha=3EI$, $\beta=K_e+v/K_B$, and $\epsilon=M_p\ell^2+J_T$. Similarly, all the elements of B are zero except b_{19}, which is K_A.

References

[1] Kelly, Pittelko, Fritz, and Forssen, Consulting Engineers, "Preliminary Feasibility Report," Terrafoil *Rapid Transit System*, Seattle, Wash., April 1971.

[2] Hartz, B.J., U.S. Patent No. 3791308, Mass Transit System, Jan. 12, 1974, U.S. Patent No. 3859925, Transportation System, Jan. 14, 1975.

[3] Hartz, B.J. and Platt, R.M., "Dynamic Response of a Rapid Transit Vehicle to Random Guideway Roughness." ASME Conf. Paper 73-ICT-15, Conference on Transportation, Boulder, Colo. Sept. 23-27, 1973.

[4] Schoenman, R.L. and Shomber, H.A., "Impact of Active Controls on Future Transport Design, Performance, and Operation," SAE Paper 751051, National Aerospace Engineering and Manufacturing Meeting, Nov. 17-20, 1975.

[5] Strahota, R.A. "Program Summary for Control Configured Vehicle Concepts Applied to Fighter Aircraft," Air Force Flight Dynamics Lab., Wright Patterson AFB, Ohio, AFFDL-TR-74-51, May 1974.

[6] Poyneer, R.E., "Design and Evaluation of a Multi-Surface Control System for the CCV B-52," *Journal of Aircraft*, Vol. 12, March 1975, pp. 135-138.

[7] Johannes, R.P. and Thompson, G.O., "B-52 Control Configured Vehicles Program," AGARD-CP-137, Geilo, Norway, Sept. 24-26, 1973.

[8] Weist, W.R., and Mitchell W.I., "The Automatic Control System for the Boeing Commercial 'Jetfoil', " *IEEE NAECON '76 Record*, Dayton, Ohio, May 18-20, 1976.

[9] Gupta, N.K. and Bryson, A.E., "Near-Hover Control of Helicopter with a Hanging Load," *Journal of Aircraft*, Vol. 13, March 1976, pp. 217-222.

[10] Asseo, S.I. and Whitbeck, R.F., "Control Requirements for Sling-Load Stabilization in Heavy Lift Helicopters," *Journal of the American Helicopter Society*, Vol. 18, July 1973, pp. 23-31.

[11] Keller, G.R., *Hydraulic System Analysis*, Ind. Pub. Co., Cleveland, Ohio, 1969.

[12] Furman, J. E., "Dynamic Modeling and Control of the Terrafoil Vehicle Under Lateral Acceleration," MSEE Thesis, University of Washington, Seattle, Wash., 1974.

[13] Luenberger, D.G., "An Introduction to Observers," *IEEE Transactions on Automatic Control*, Vol. AC-16, Dec. 1971, pp. 596-602.

[14] Fath, A. F., "Computational Aspects of the Linear Optimal Regulator Problem," *IEEE Transactions on Automatic Control*, Vol. AC-16, Oct. 1969.